Advanced Virgo and beyond

a journey in the exploration of space-time with Interferometric Gravitational Wave Detectors

INFN Seminar – Pisa, April 28, 2021

Francesco Di Renzo – Physics Department of Pisa University
francesco.direnzo@df.unipi.it

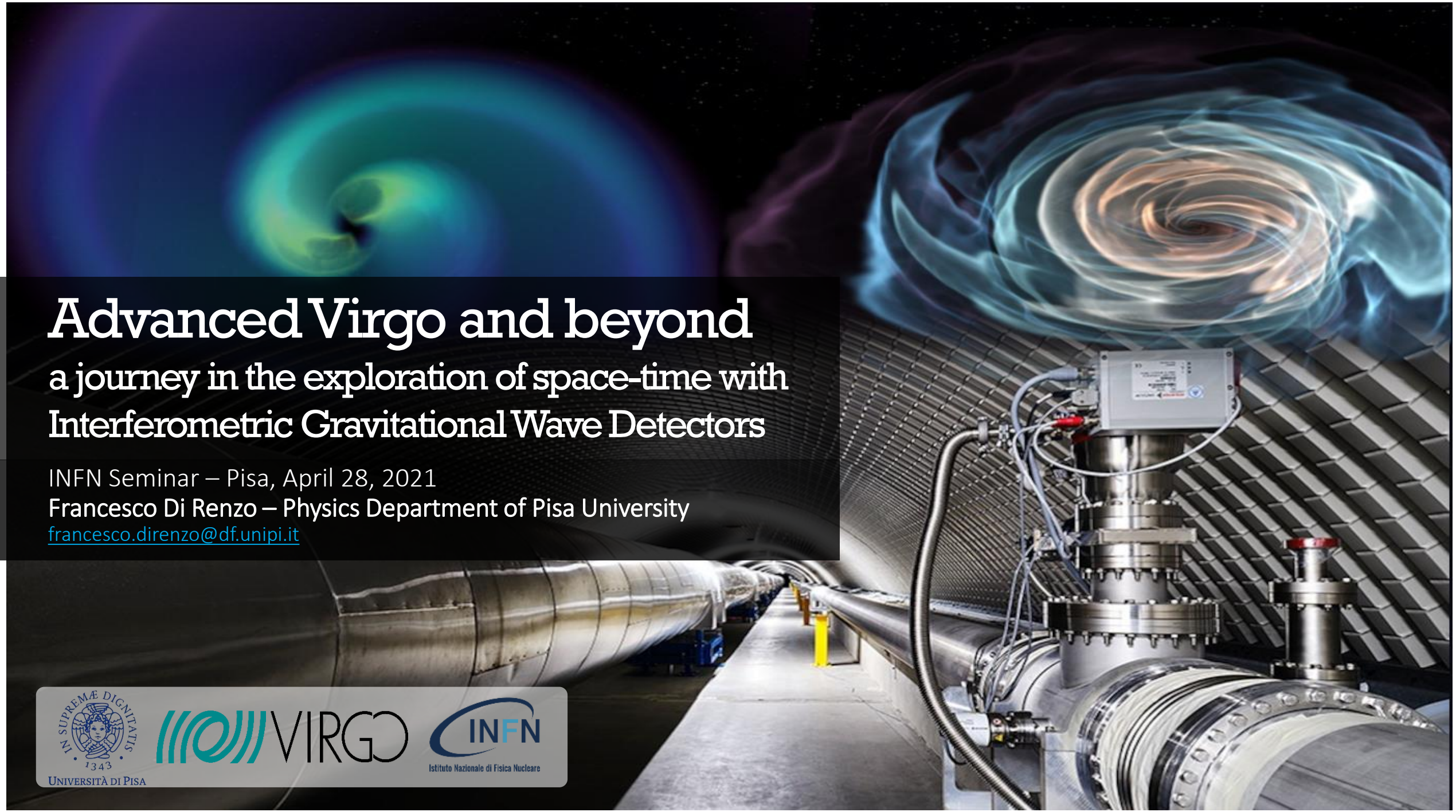

Exploring space-time: from O1 to O3b

Effective Binary Neutron Star (BNS) Volume-Time explored vs the number of compact binary coalescence (CBC) detections:

Observing runs:

O1: Sep 12, 2015 – Jan 19, 2016

O2: Nov 30, 2016 – Aug 25, 2017

O3a: Apr 1, 2019 – Oct 1, 2019

O3b: Nov 1, 2019 – Mar 27, 2020

Some key events:

GW190814
GW190521
GW190425
GW170817
GW170814
GW150914

LIGO-G1901322/public

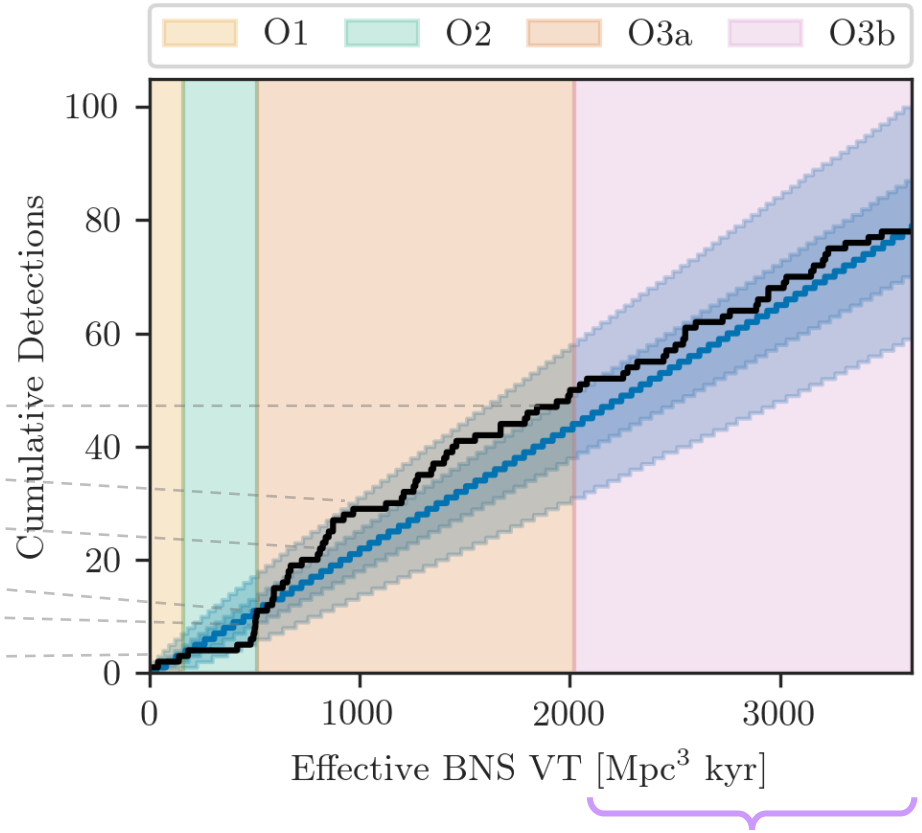

non-retracted public alerts

The rate density of compact binary coalescences

Compact binary star systems can emit detectable Gravitational Waves (GW) in the last stages of their inspiral motion.

- **BNS**: two Neutron Stars (NSs) system, *e.g.* GW170817;
- **NSBH**: binary formed by one Neutron Star and one Black Hole (BH);
- **BBH**: two Black Holes (BHs) system, *e.g.* GW150914.

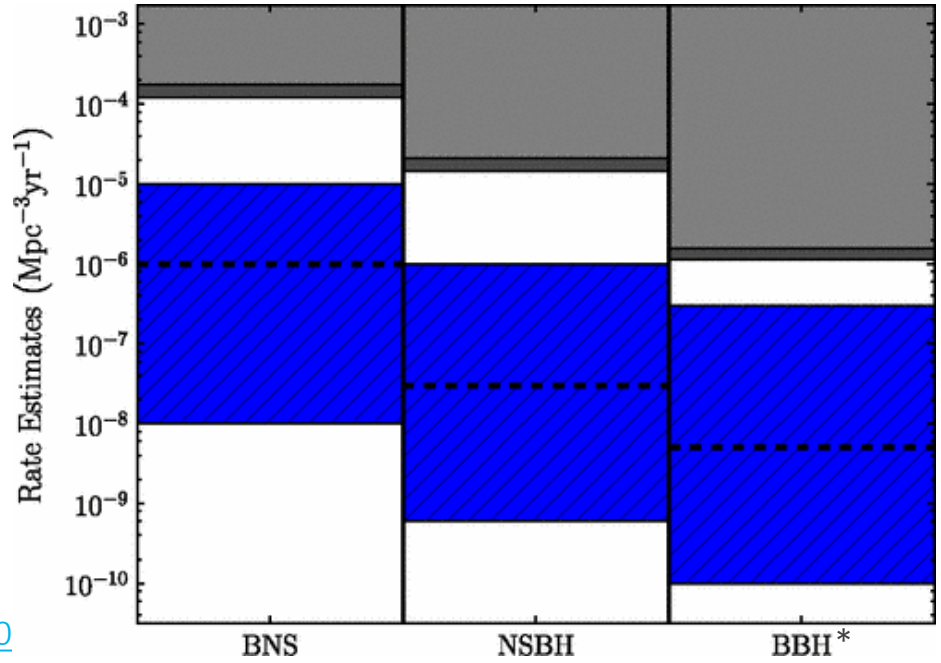

Abadie2010

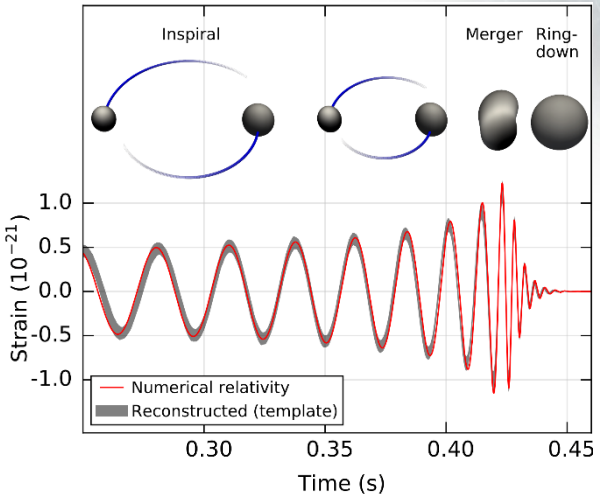

PhysRevLett.116.061102

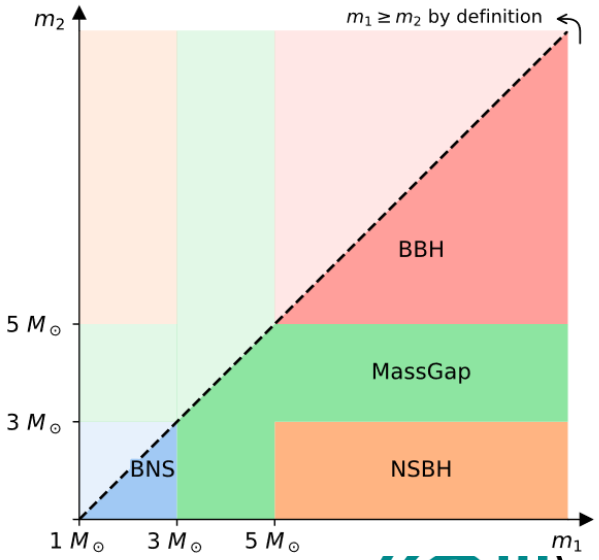

Abbott2013

*Updated inference on BBH population arXiv2010.14533

Quantifying the detector performance

The detector **strain sensitivity** is the minimum *detectable* value of the strain produced by an incoming GW:

⇒ It is determined by the **detector noise**.

BNS inspiral range: the distance, averaged over GW polarizations and directions in the sky, at which a single detector can observe with matched-filter Signal-to-noise Ratio (SNR) of 8 the inspiral of two neutron stars.

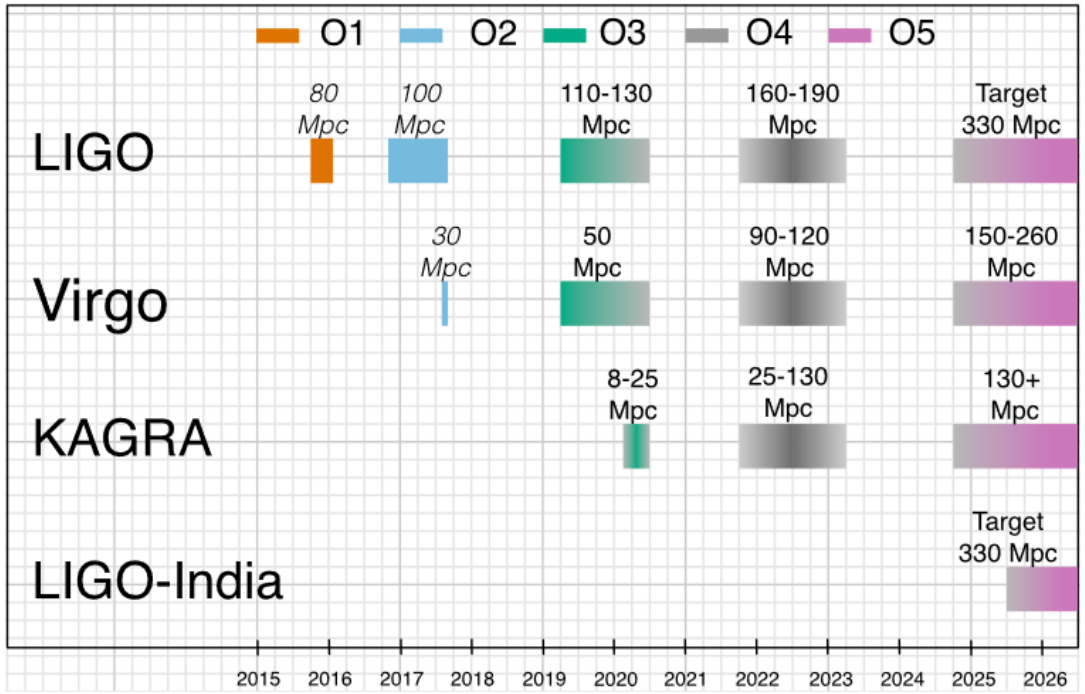

[Abbott2013]

Mass distribution of Galactic binary neutron stars [Farrow2019]

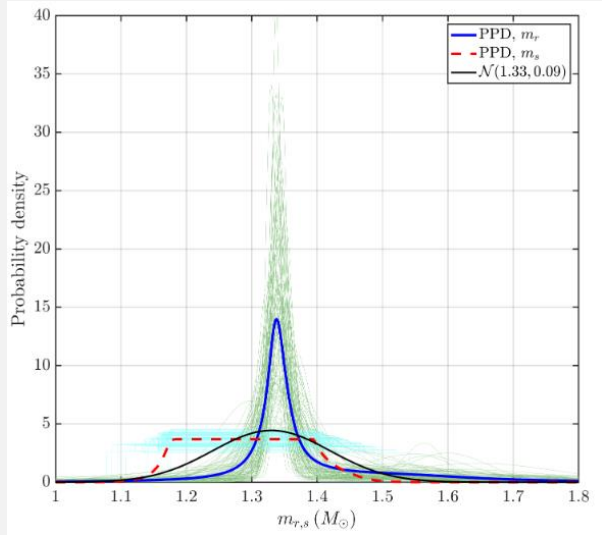

The effective BNS Volume-Time

Euclidean sensitive volume of the second-most sensitive detector in the network at a given time, multiplied by the **live time** of that network configuration.

The **network Euclidean sensitive volume** is the volume of a sphere with a radius given by the **BNS inspiral range.**

⇒ Multiplying the BNS Volume-Time by the **CBC density rate** we get an estimate of the expected number of detections. (ignoring cosmological corrections)

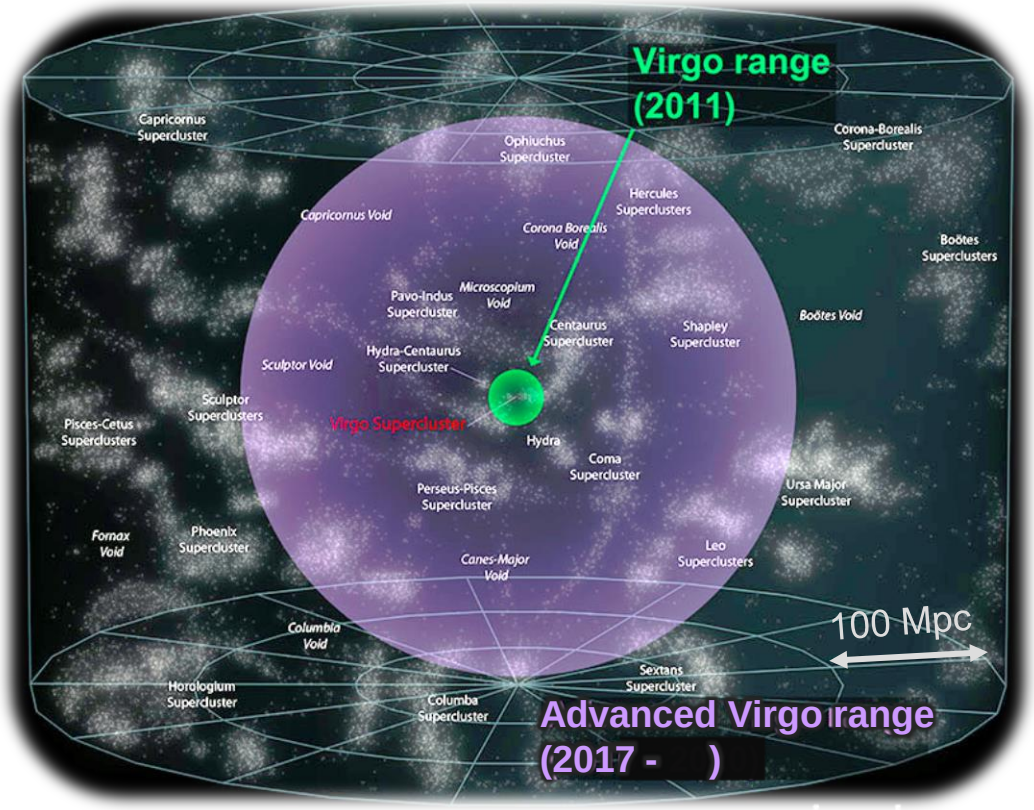

Image Credit: Virgo Collab.

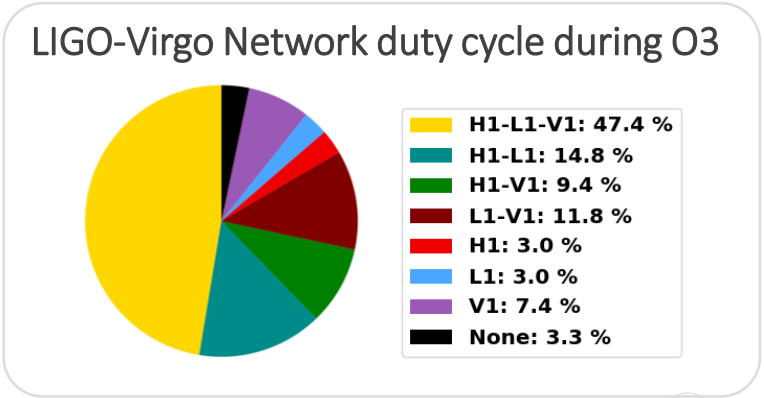

Increase in BNS range from O2 to O3a

Gravitational Wave Transient Catalog (GWTC): updated lists with all the GW transient detections are regularly published in the forms of catalogs.

GWTC-1: O1 - O2

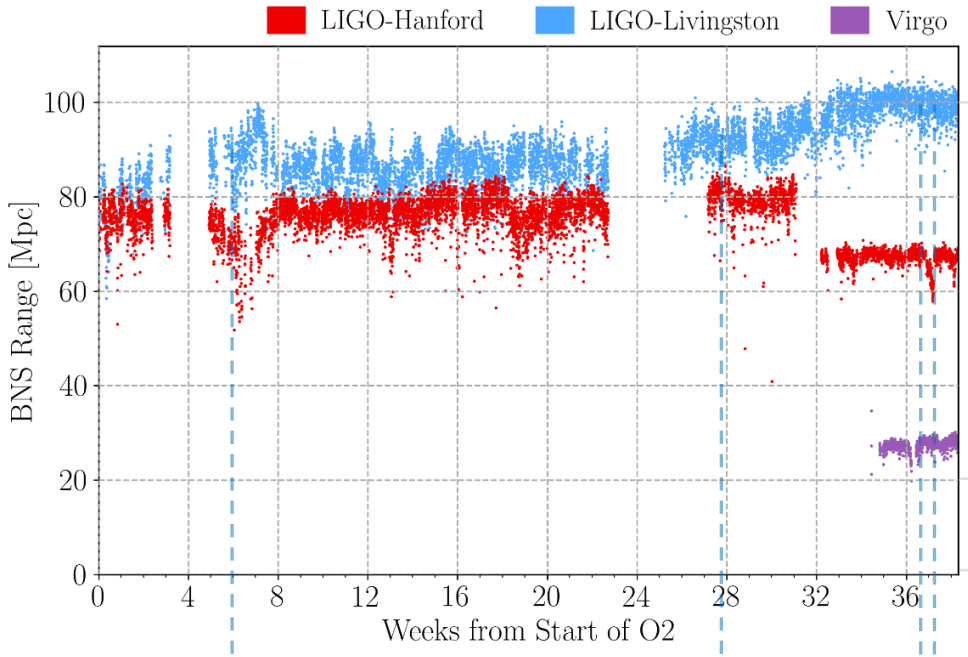

GWTC-2: O1 - O3a

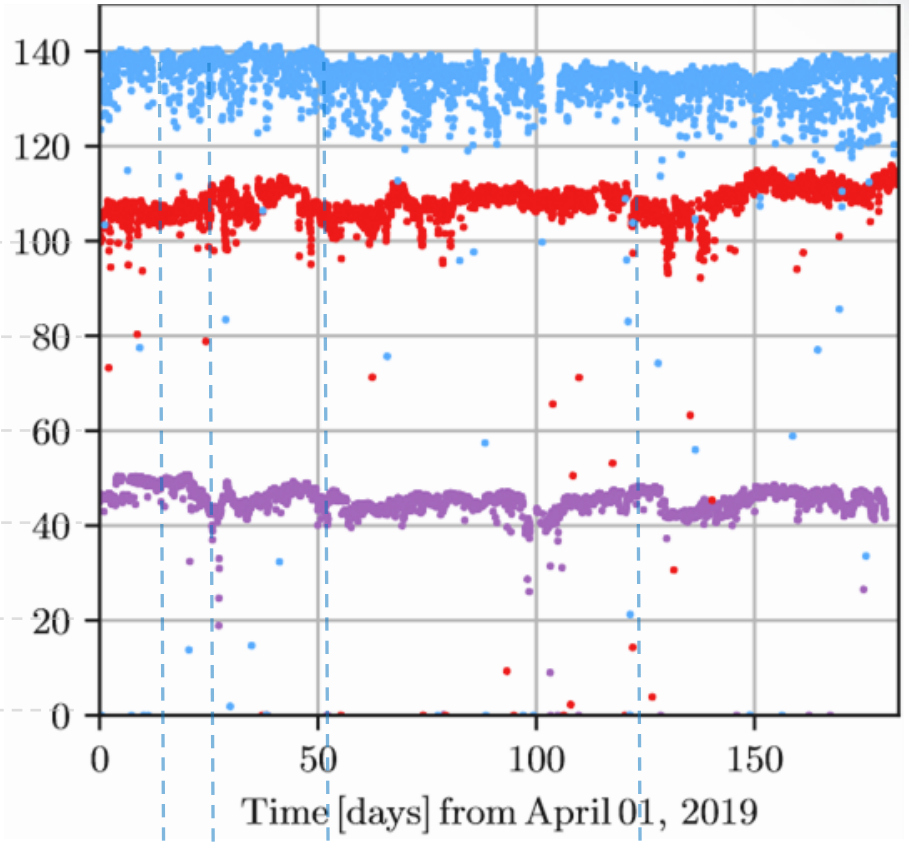

Frequency dependent strain sensitivity

Detector noise is conveniently described as a **stochastic process.** Its dominant contributions can be overall assumed to be **stationary and Gaussian**.

⇒ Its statistical properties are fully characterized by its **correlation matrix**, or, equivalently**,** by the **Power Spectral Density (PSD);**

⇒ Its Amplitude Spectral Density (ASD, square root of the PSD) provides a frequency-dependent measure of the detector sensitivity.

Noise sources and limitations to the sensitivity

- Fundamental noises: from the physical limitation of the detection principle and its implementation (continuous lines);
- Technical noises: from the actual implementation of the detector with components that are *not optimal*, have imperfections (dashed lines, only for ~stationary ones);
- Environmental noise, everything not included in the previous categories, usually originating from the outside of the detector.

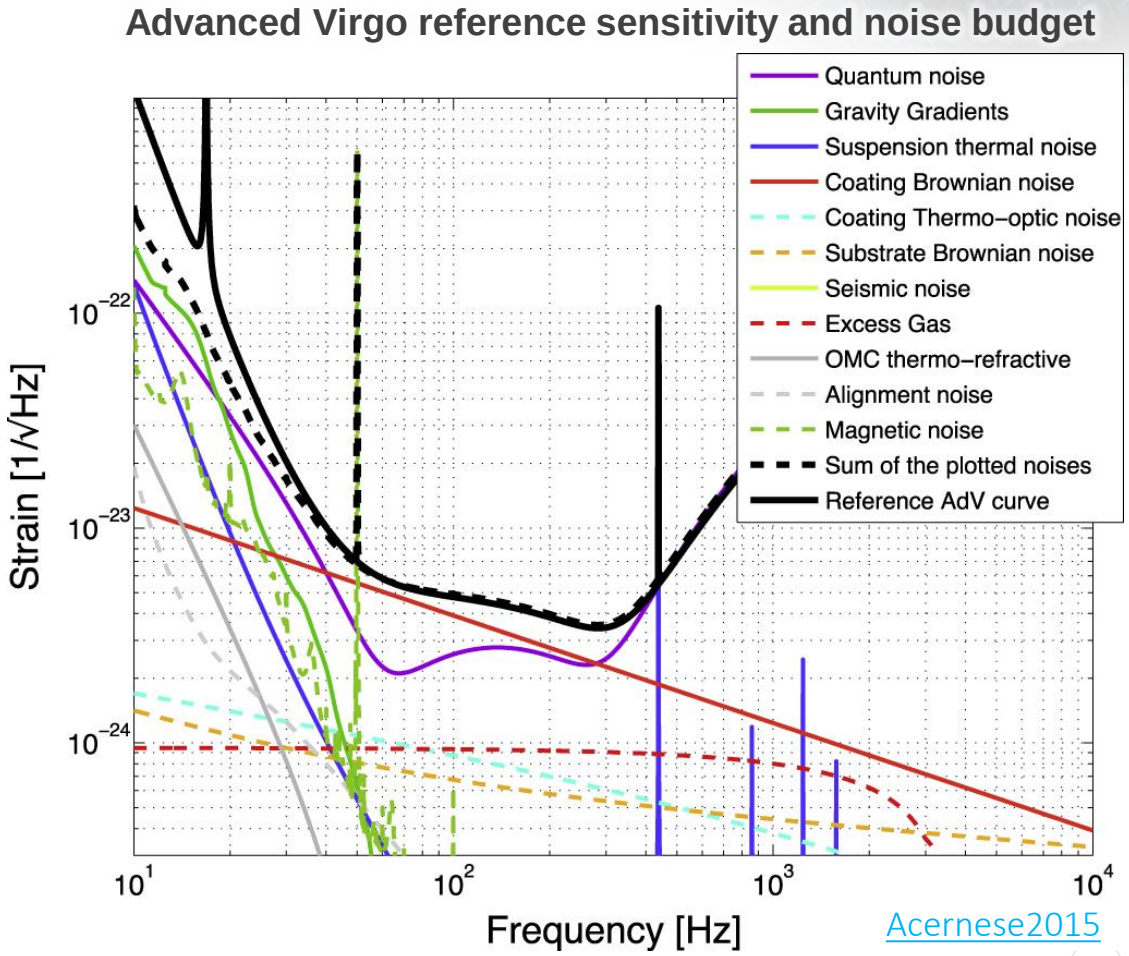

Acernese2015

Detector sensitivities and their evolution

- "Spikes" (spectral lines) in the strain sensitivity include technical noises not included in the noise budget at the previous page;
- "Bumps" are usually a symptom of **non-stationary** or **non-linear** contributions to the noise.

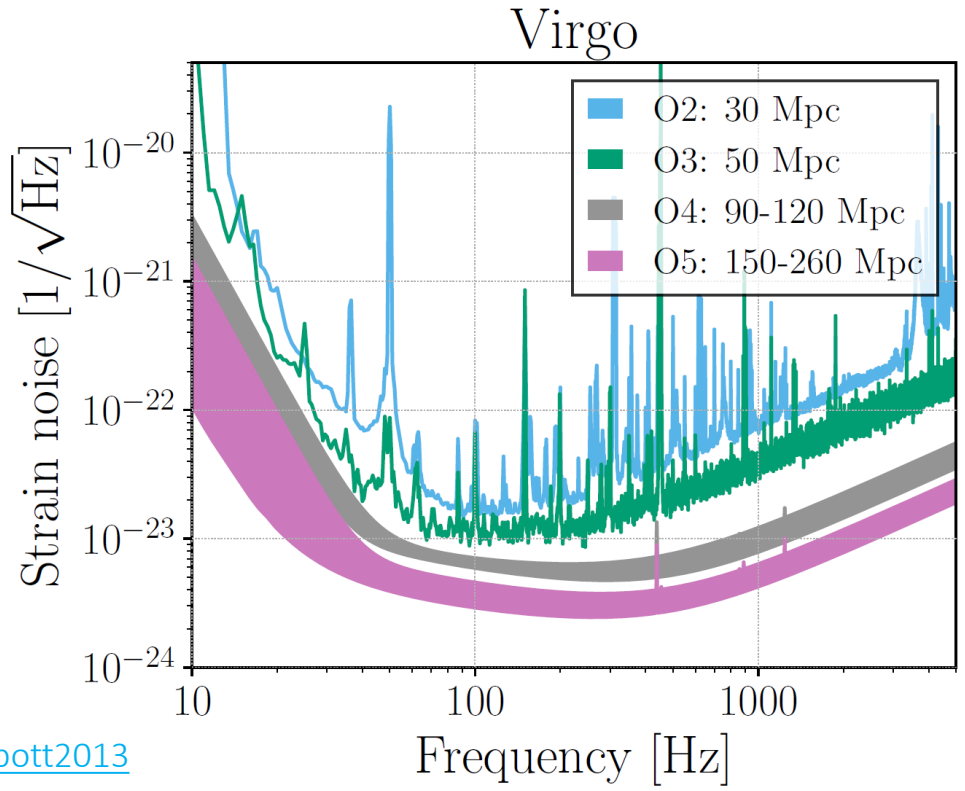

[Abbott2013]

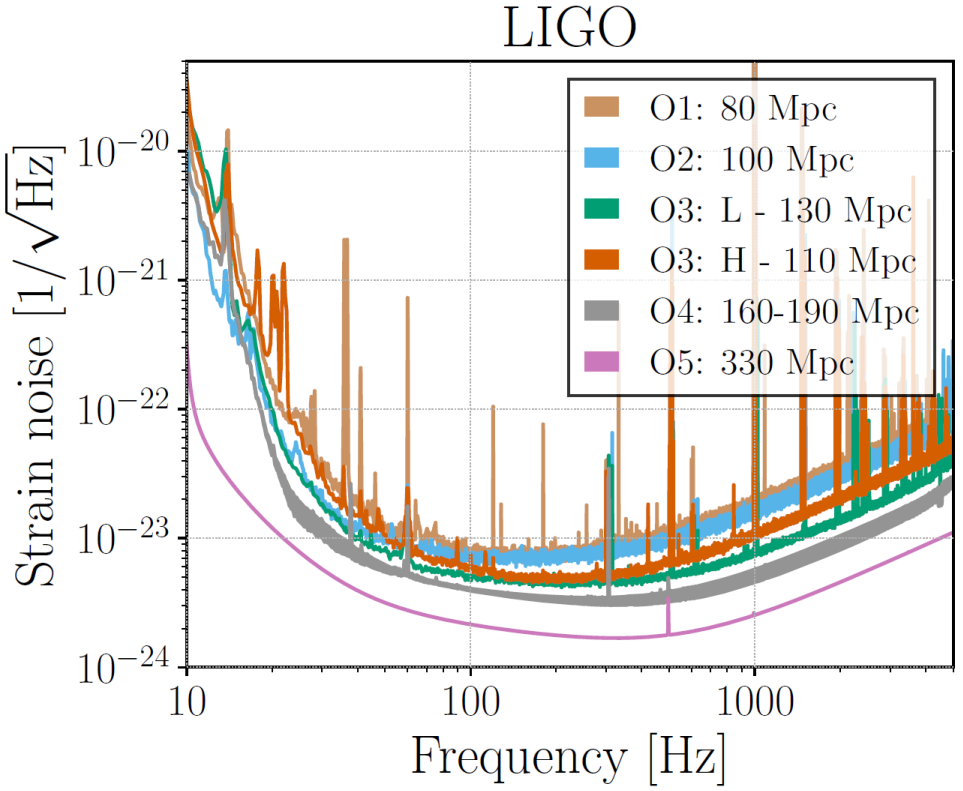

Advanced Virgo sensitivity from O2 to O3b

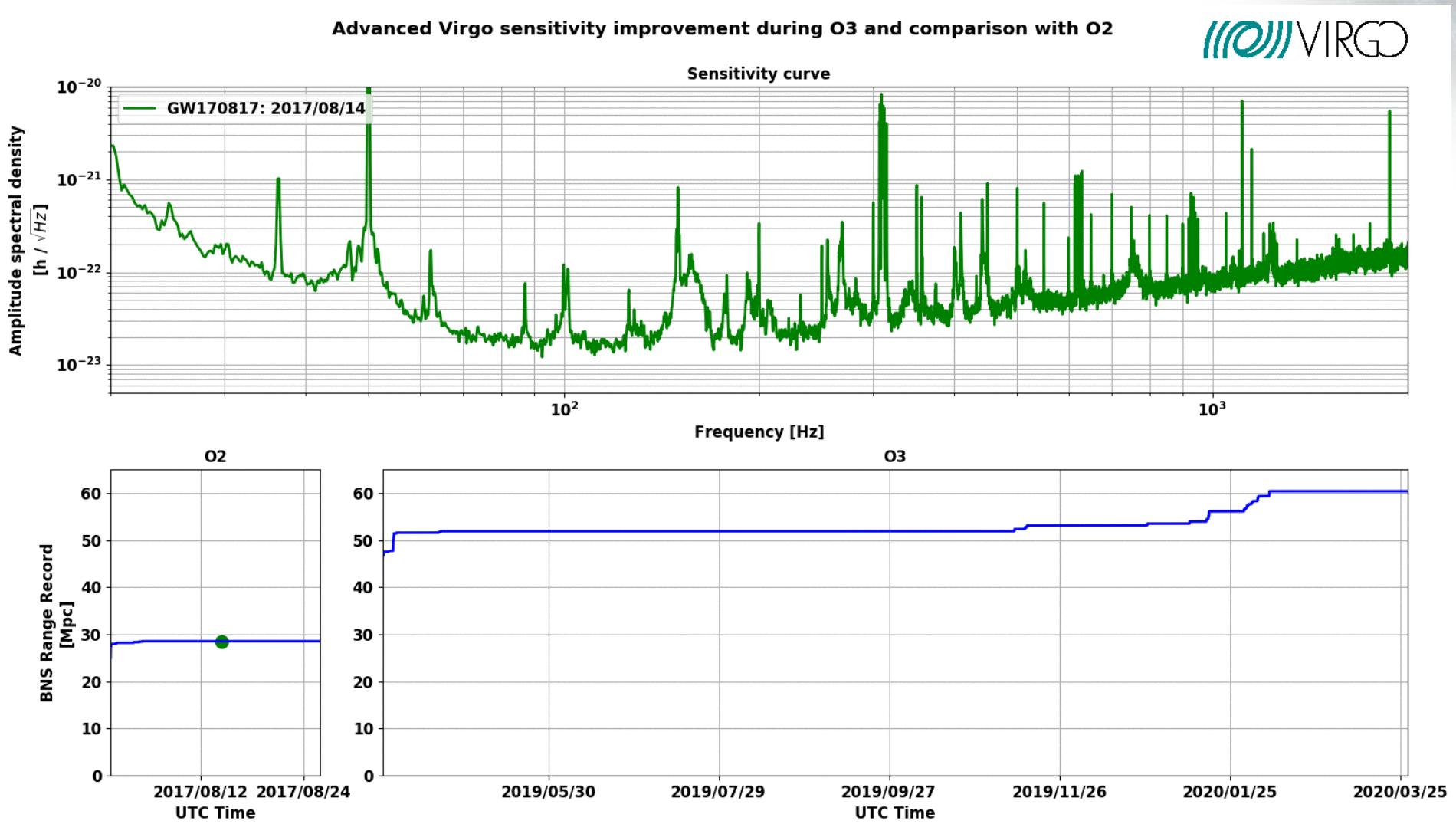

VIR-0462A-20

The matched filter technique and the BNS range

Additive noise model:

$$\underbrace{x(t)}_{\text{detector data}} = \underbrace{n(t)}_{\text{noise}} + \underbrace{s(t)}_{\text{signal}}$$

Signal model:

$$s(t) \approx \varrho h(t)$$

with ϱ the amplitude and $h(t) = h(t;\boldsymbol{\theta})$ the waveform model ($(\boldsymbol{h}|\boldsymbol{h}) = 1$).

Optimal detection statistic: likelihood ratio, in stationary and Gaussian noise equivalent to:

$$(\boldsymbol{x}|\boldsymbol{h}) = 4\,\Re\int_0^\infty \frac{\tilde{x}(f)\tilde{h}^*(f)}{S(f)}\,df$$

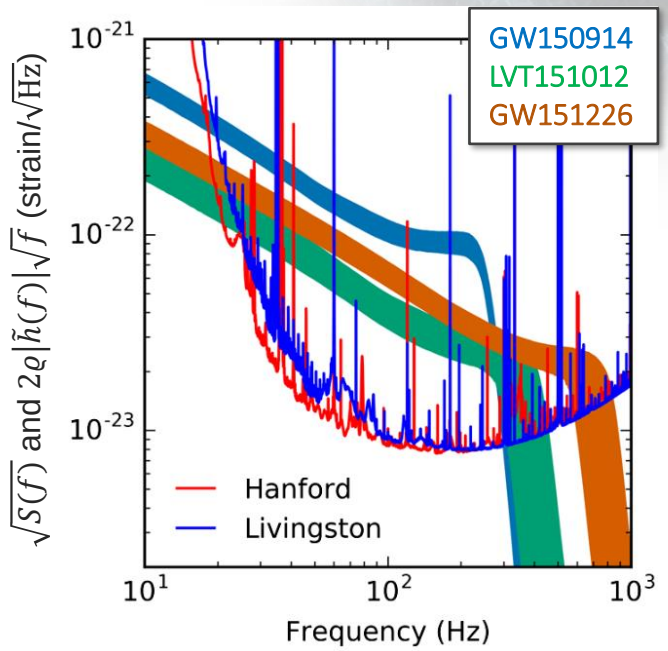

Phys. Rev. X 6, 041015

Compact binary inspiral range [Bassan2014]:

$$\frac{d_{\text{range}}}{1\ \text{Mpc}} = \frac{1}{2.26} \times 1.95 \times 10^{-20} \left(\frac{\mathcal{M}}{M_\odot}\right)^{5/6} \sqrt{\int_{f_{\text{min}}}^{f_{\text{ISCO}}} \frac{f^{-7/3}}{S(f)}\,df}$$

where $f_{\text{ISCO}} \approx 4.4\ \text{kHz}\ \left({}^{M_\odot}/_{M}\right)$. For two NS of $1.4M_\odot$: $\mathcal{M} \approx 1.22\ M_\odot$ and $f_{\text{ISCO}} \approx 1.57\ \text{kHz}$.

Simplified optical layout of the Virgo detector

The Virgo detector is a power-recycled, modified **Michelson interferometer** that exploits Fabry-Pérot cavities in its arms.

- The Michelson configuration is optimal for detecting the *differential variations* induced by an incoming GW on its arms;
- High power laser source: Nd:YAG of 1064 nm wavelength;
- Main optics constituted of a bulk of fused silica and high-quality coatings;
- All test mass mirrors are suspended through a chain of mechanical filters plus an inverted pendulum called *Superattenuator* [Braccini2005];
- Fabry-Pérot cavities increase the optical path of the light along the two arms by a factor proportional to the *finesse*. Sensitivity increases by a similar factor at high frequency;
- A suspended power recycling mirror creates a further optical cavity with the bright port of the beam splitter: increases circulating power [VIR-0128A-12].

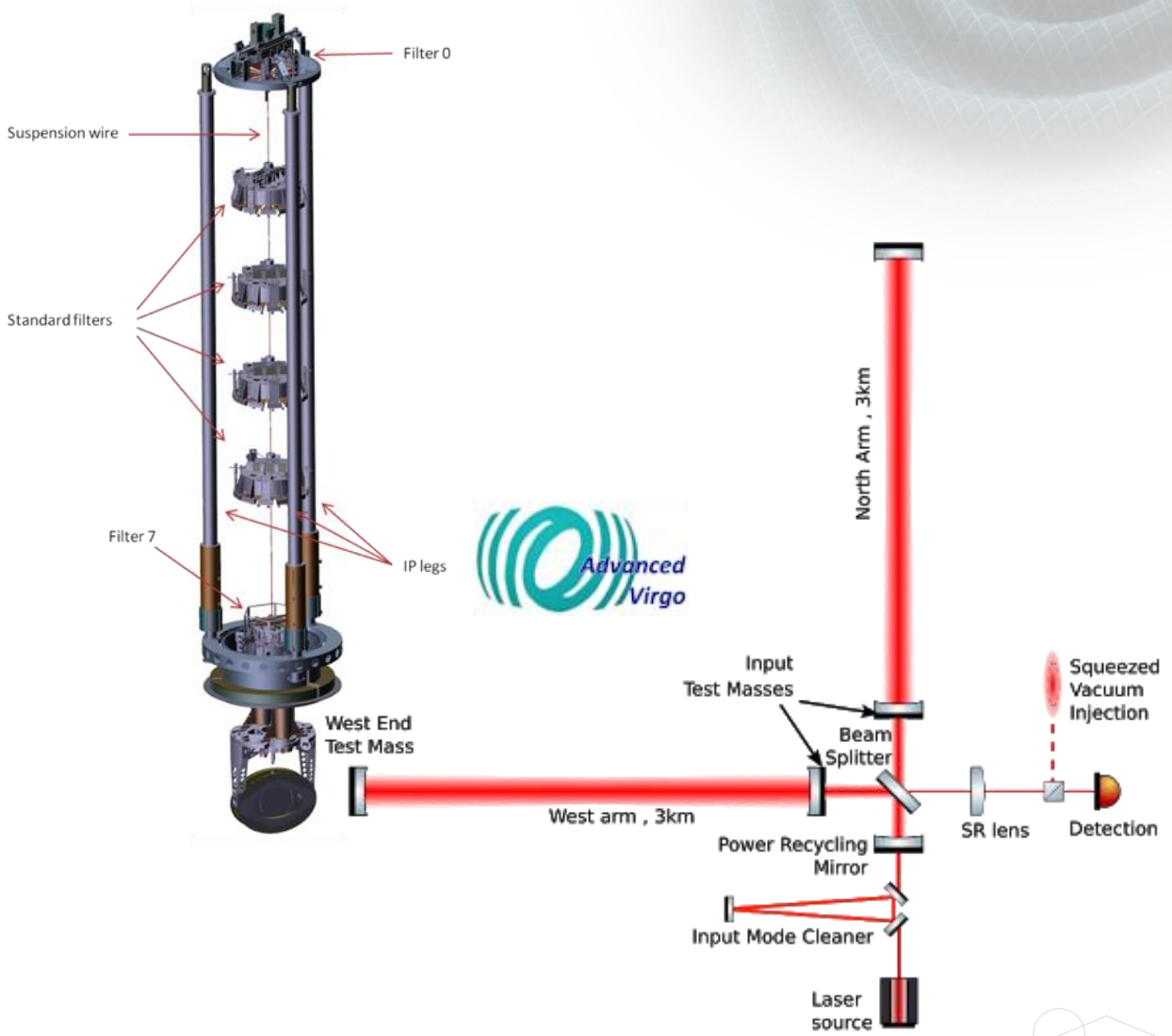

From Virgo to Advanced Virgo

Advanced Virgo project started in 2011, with the goal of increasing the BNS range by one order of magnitude:

→ 1000 times larger sensitive volume (and detections).

Main upgrades before O2 [Acernese2015]:

- Heavier mirror test masses: from 20 kg to 42 kg;
- Thermal Compensation System to compensate defects of core optics due to laser heating: Ring Heaters, Compensation Plates. New payload design;
- Larger beams at input test mass mirrors: from 2.4 cm to 6 cm;
- Better optics: finesse 3 times larger, improved coatings to reduce losses (absorption and scattering);
- Suspended optical benches in vacuum for the injection and detection optics, new set of baffles and diaphragms: reduce *scattered light* from vibrating surfaces

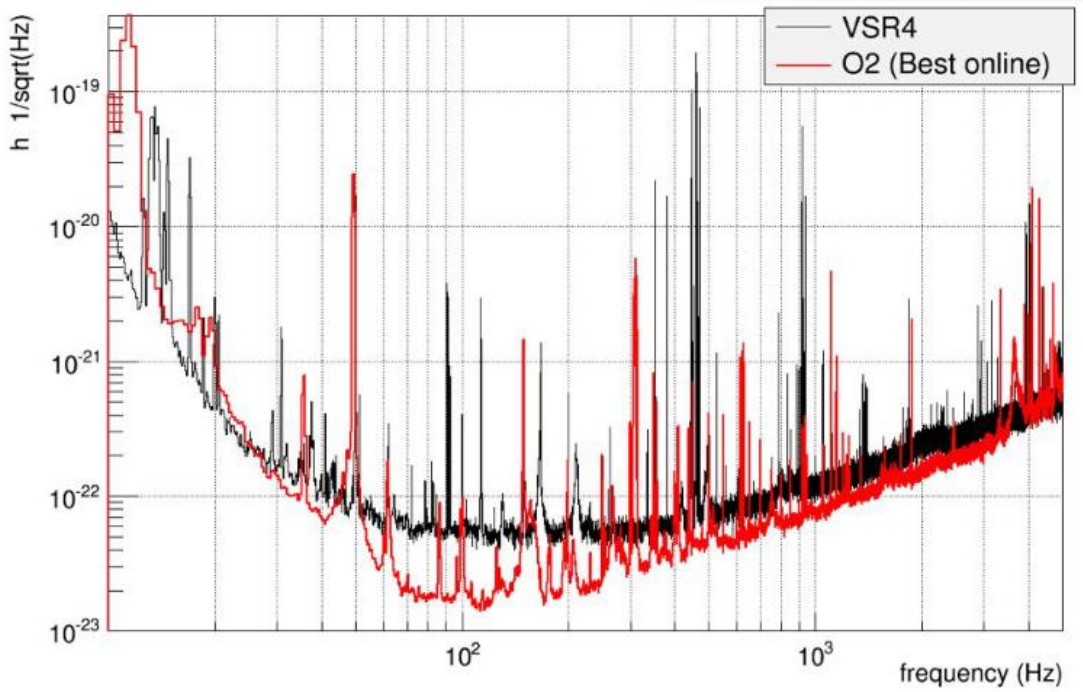

Virgo+ (2011): 12 Mpc → Advanced Virgo (O2): 30 Mpc

Advanced Virgo from O2 to O3a

Upgrades between O2 and O3a:

- Replacement of the steel wires suspending the four test masses with fused-silica, monolithic suspensions: reduction of suspension thermal noise below 100 Hz [Aisa2015];
- More powerful laser (65 W), which increased from 10 to 19 W the injected power, improving both stability and high frequency sensitivity;
- (Frequency independent) squeezed light injection. Reduction of shot noise, slight increase in radiation pressure below 40 Hz [Acernese2019];
- Subtraction of 50 Hz mains line and improved control strategy for the suspended benches below 30 Hz;
- Identification and mitigation of several other sources of technical and environmental noise: less spectral lines and noise features.

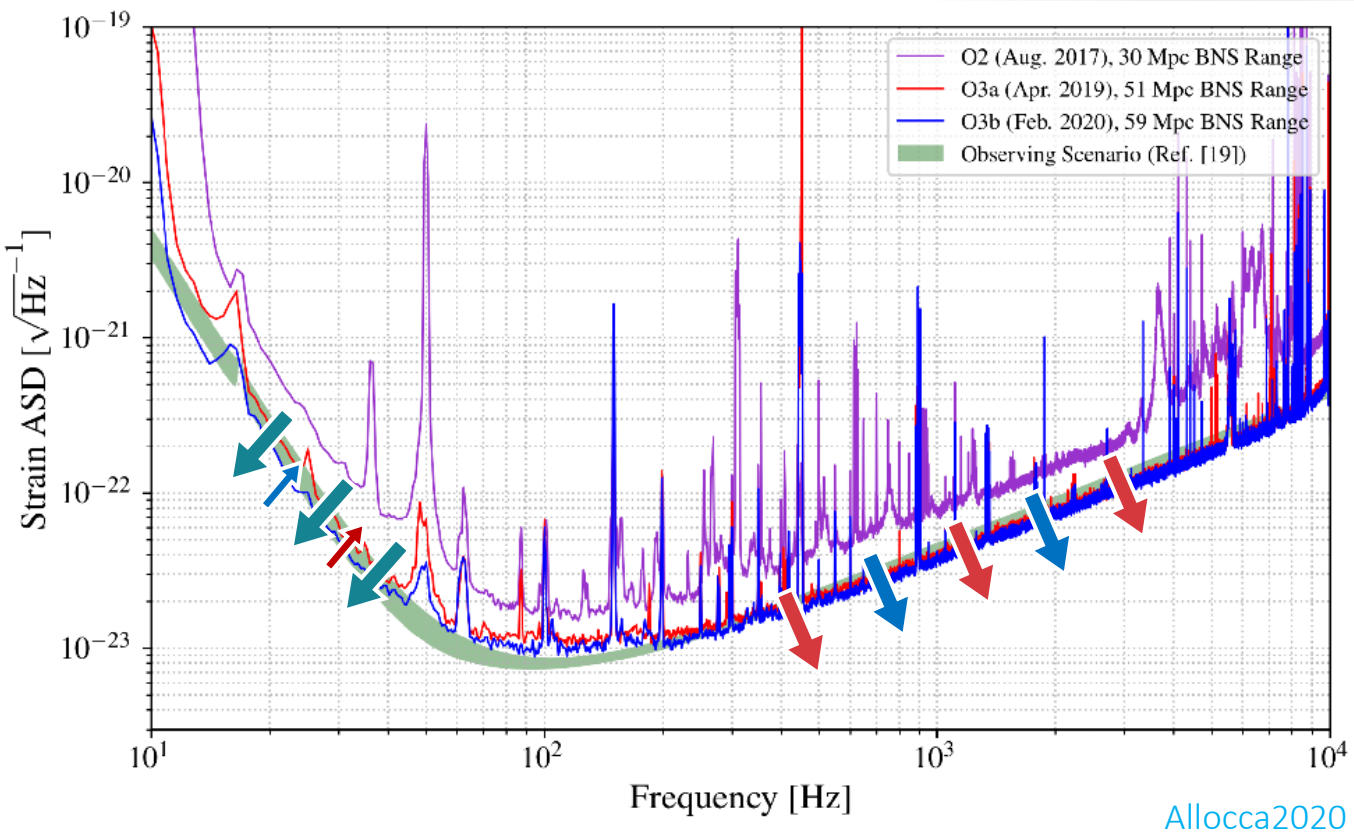

Allocca2020

Advanced Virgo from O3a to O3b

Upgrades between O3a and O3b:

- Increase of the laser power to 26 W;
- Replacement of some pre-amplifiers of the detection photodiodes: removal of flicker noise and +2 Mpc increase from January 2020;
- Improved performance of the *etalon feedback system*: reduction of residual finesse asymmetry by acting on the mirror temperature. +2-3 Mpc of BNS range [Brooks2020];
- Software modifications to the reconstruction of the strain signal (*hrec*): +2 Mpc promoting some channels from single to double precision;
- Mitigation of some scattered light sources related to the alignment of the squeezing.

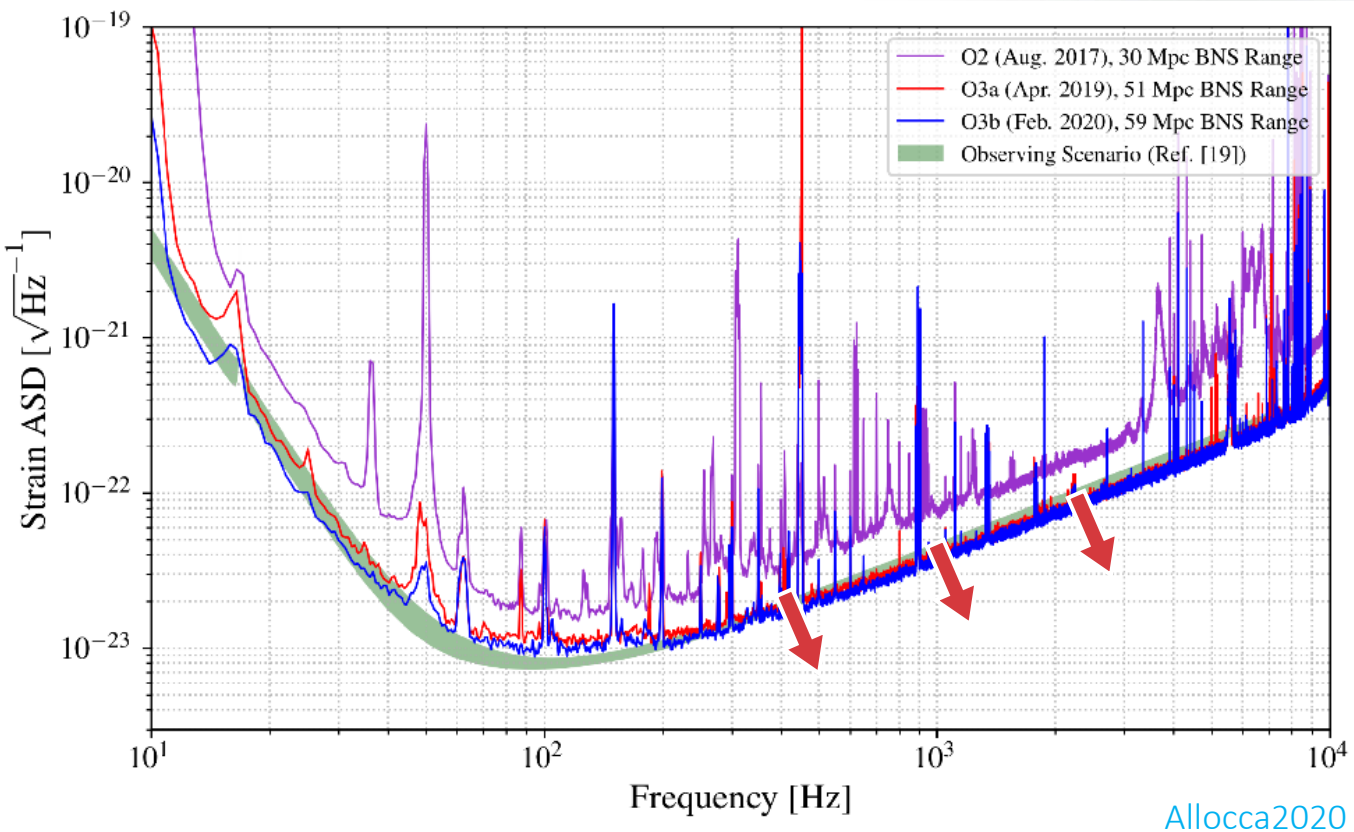

Allocca2020

Reduction of non-stationary noise

So far, we have mostly dealt with the improvement of the sensitivity from the point of view of the stationary and Gaussian part of the noise. Also the rate of transient excesses of power (*glitches*) has been significantly reduced:

- From O2 to O3a: **reduction by 40 times** of the glitch rate per minute;
- From O3a to O3b: increase by 60%, mostly due to bad weather conditions associated to seasonal change.

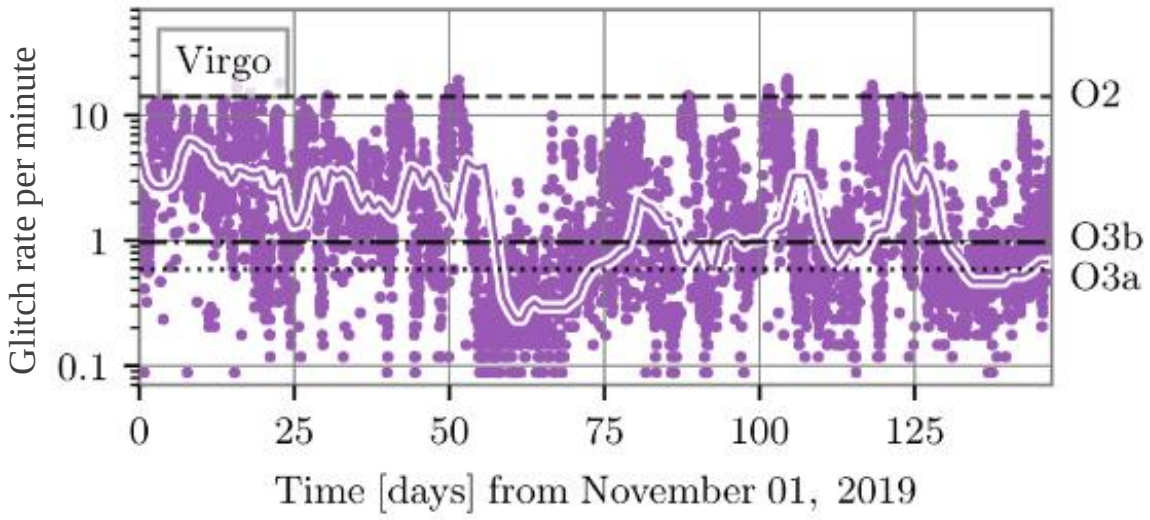

Example of Scattered light glitch

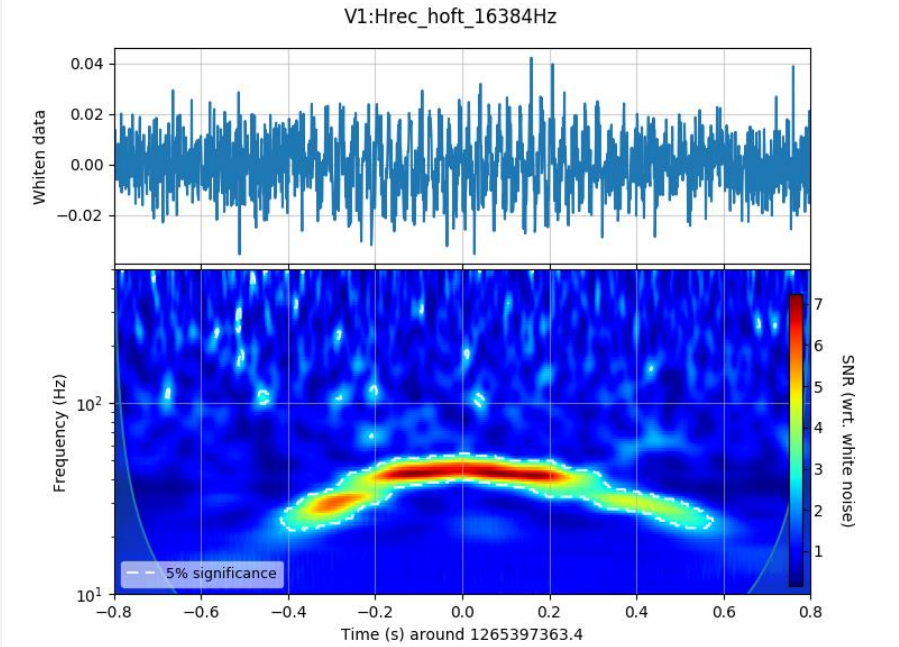

Advanced Virgo+: phase I, 2020-2022

Goal: reduction of quantum noise, reach 100 Mpc for O4

- **Signal recycling** mirror (installed July 2020): reinject signal into the interferometer. By varying the resonance condition, it is to "tune" the detector sensitivity [Danilishin2019];
  - Auxiliary green laser system to control FP cavities: now 5 longitudinal d.o.f.;
- **Frequency dependent squeezing** (infrastructure ready early 2021): squeezed light with different angles depending on the frequency. Reduce shot noise at high frequency and radiation pressure at low frequency;
- **New laser system** (2020 completed): 100 W monolithic fibered system, able to inject ~75 W in the interferometer (65 W done);
- New **payload** and **end-mirror** replacement for the **Input Mode Cleaner** cavity (2020 completed). Baffle installation (ongoing);
- High finesse Output Mode Cleaner (2020 completed). Reduce losses and mitigate scattered light with diaphragms and beam dumps;
- **Newtonian Noise Cancellation** (installation completed, ongoing characterization): array of seismic sensors around the main mirrors.

VIR-0168F-21

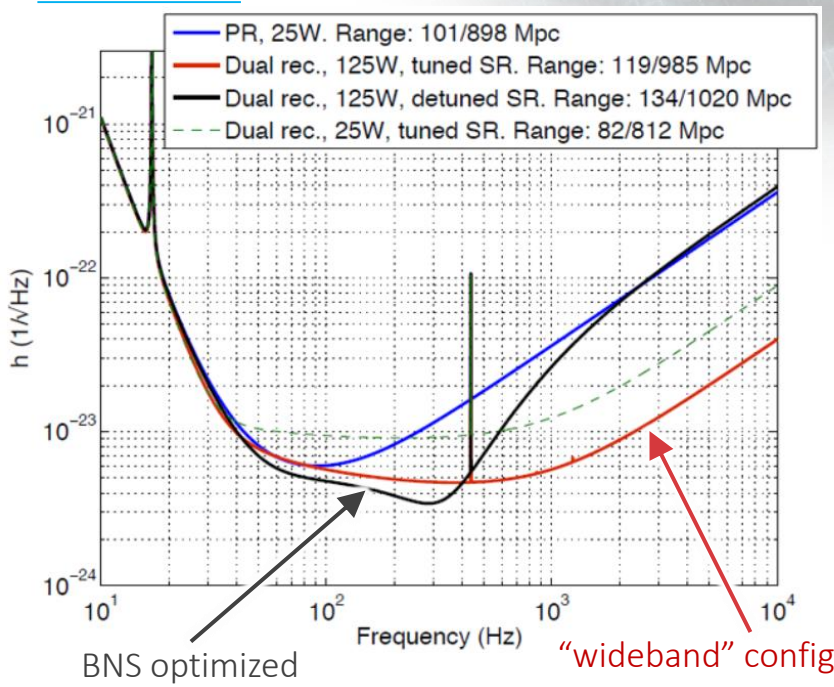

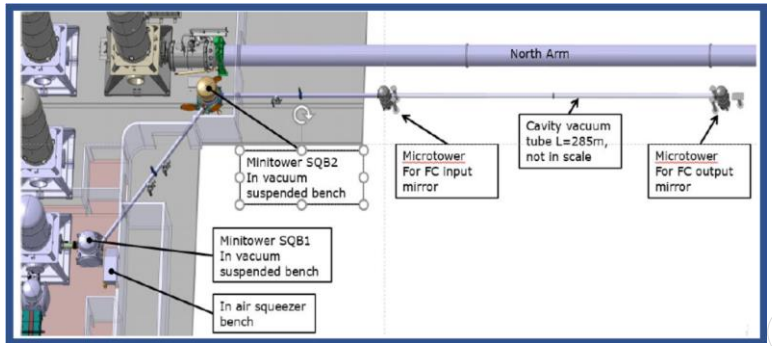

Advanced Virgo+: phase II, 2023-2025

towards the limits of 2nd generation detectors

Goal: reduce thermal noise, reach 200 Mpc

- Modified beam geometry inside arm cavities to increase the beam size on the end mirrors: larger area, smaller thermal noise effects, in particular around 100 Hz;
  - Larger test masses (40 → 105 kg, 35 → 55 cm diameter);
  - New suspensions and seismic insulation mechanisms;
- New coatings with lower mechanical losses: expected reduction by a factor 3;
  - New materials to be identified before August 2021. Possible candidates:
    - Silicon Nitride,
    - Gallium Nitride.

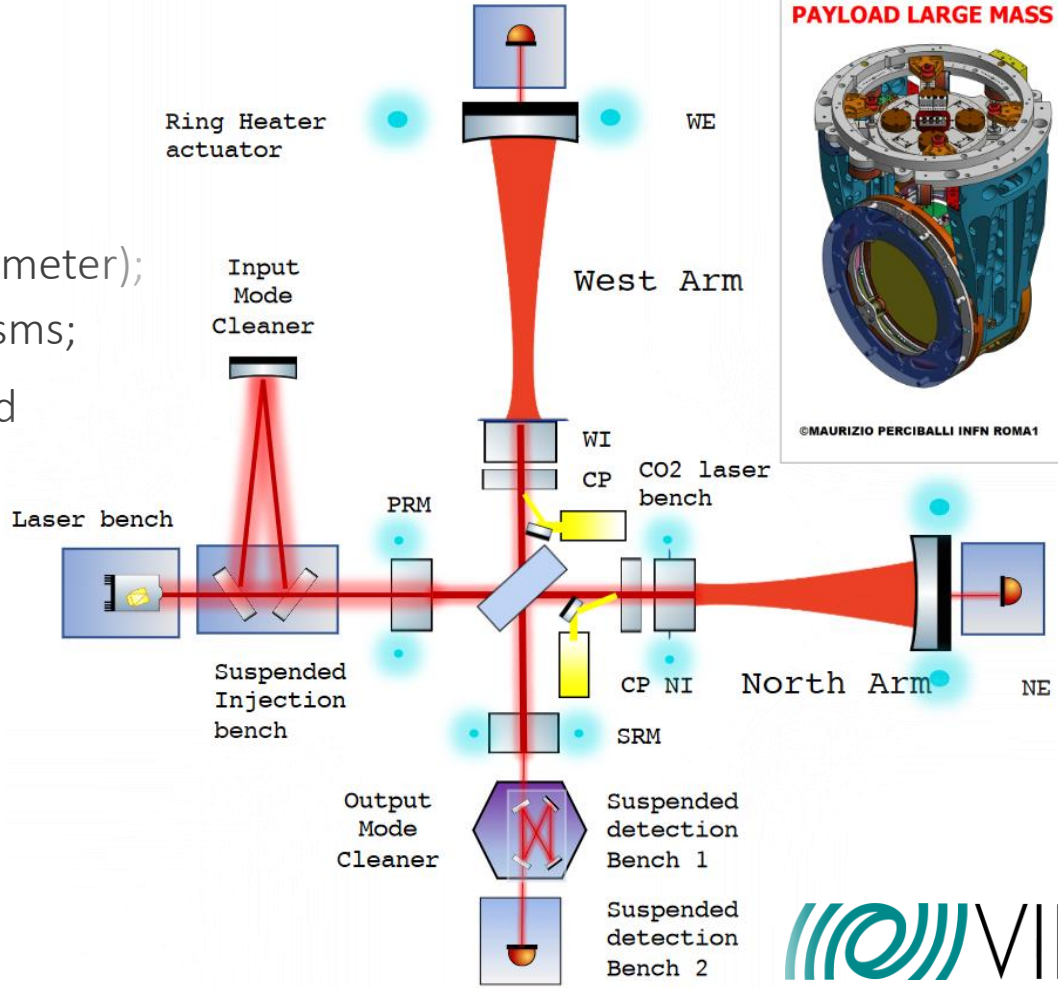

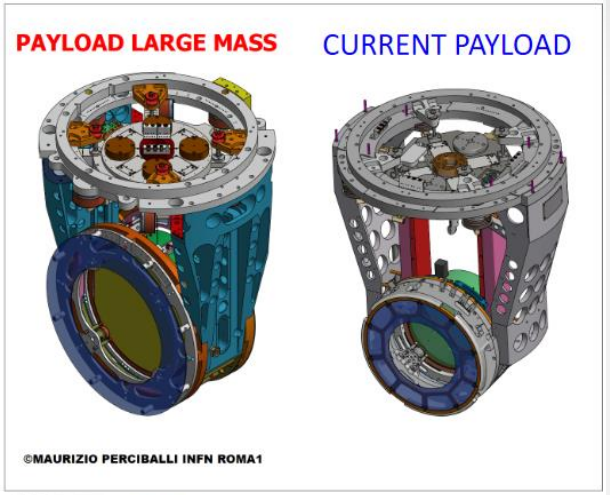

Advanced Virgo+ design sensitivity

Main parameters of Advanced Virgo+ for phase I and phase II [Flaminio2020]:

Parameter	O4 high	O4 low	O5 high	O5 low
Power injected	25 W	40 W	60 W	80 W
Signal recycling	Yes	Yes	Yes	Yes
Squeezing type	FIS	FDS	FDS	FDS
Squeezing detected level	3 dB	4.5 dB	4.5 dB	6 dB
ITM mass	42 kg	42kg	42 kg	42kg
ETM mass	42 kg	42kg	105 kg	105kg
ITM beam radius	48.7 mm	48.7 mm	48.7 mm	48.7 mm
ETM beam radius	58 mm	58 mm	96 mm	96 mm
Coating losses ETM	2.37e-4	2.37e-4	2.37e-4	0.79e-4
Coating losses ITM	1.63e-4	1.63e-4	1.63e-4	0.54e-4
Newtonian noise reduction	None	1/3	1/3	1/5
Technical noise	"Late high"	"Late low"	"Late low"	None
BNS range	90 Mpc	115 Mpc	145 Mpc	260 Mpc

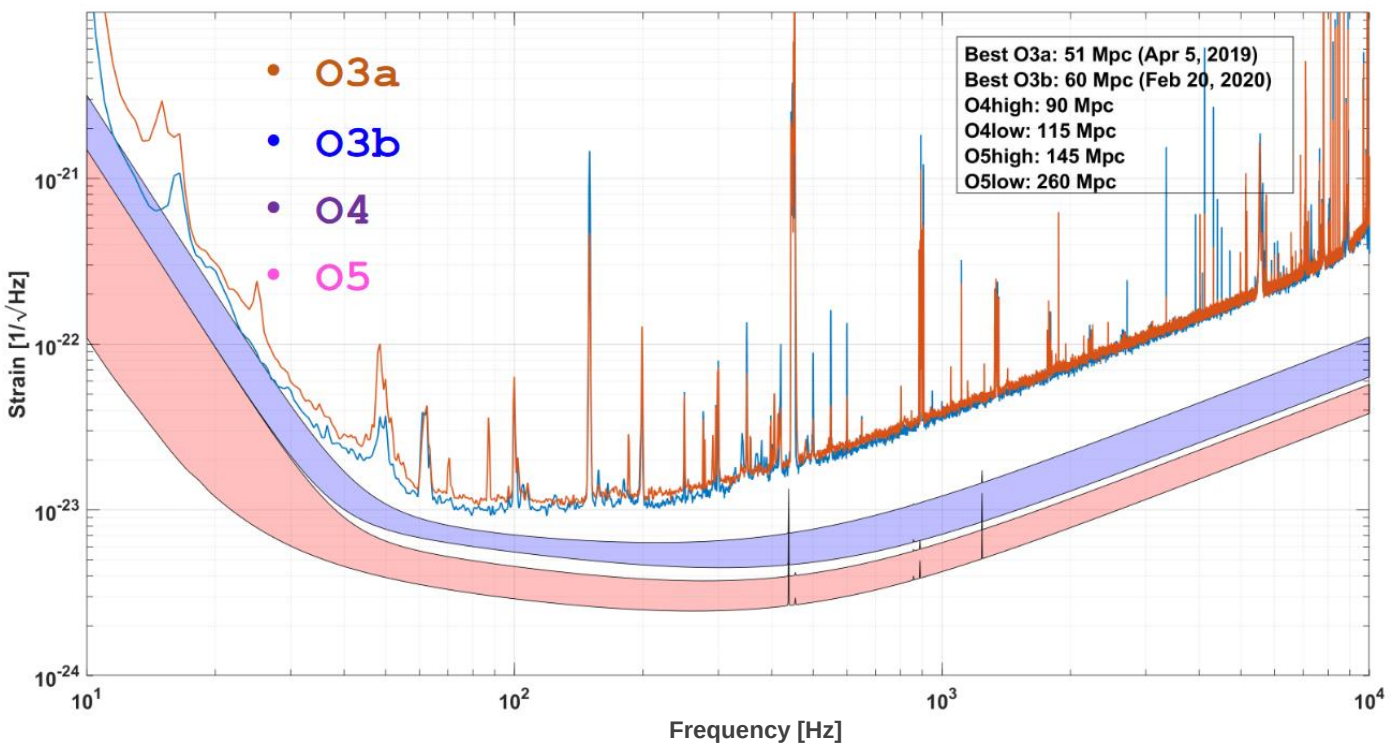

high: pessimistic case, non-optimal configuration
low: best sensitivity goal

3rd generation detectors: the Einstein Telescope

Goal: achieve sensitivities 100 times better than 1st gen. detectors

- Located underground to reduce seismic and Newtonian noise;
- 10 km long arms, in an equilateral triangle configuration: able to resolve GW polarizations;
- Xylophone configuration: each of the three detectors would be composed of two interferometers, one optimized for operation below 30 Hz and one optimized for operation at higher frequencies;
- The low-frequency interferometers will use cryogenic optics, cooled to 10 K, with a beam power of about 18 kW in each arm cavity. The high-frequency ones (10 Hz to 10 kHz) will use room-temperature optics and a much higher recirculating beam power of 3 MW.

[ET conceptual design study]

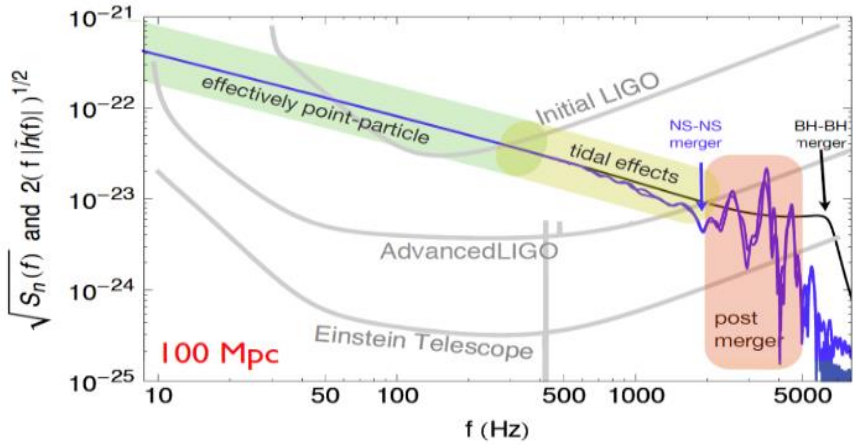

Image credit: Michele Maggiore et al JCAP 03(2020) 050

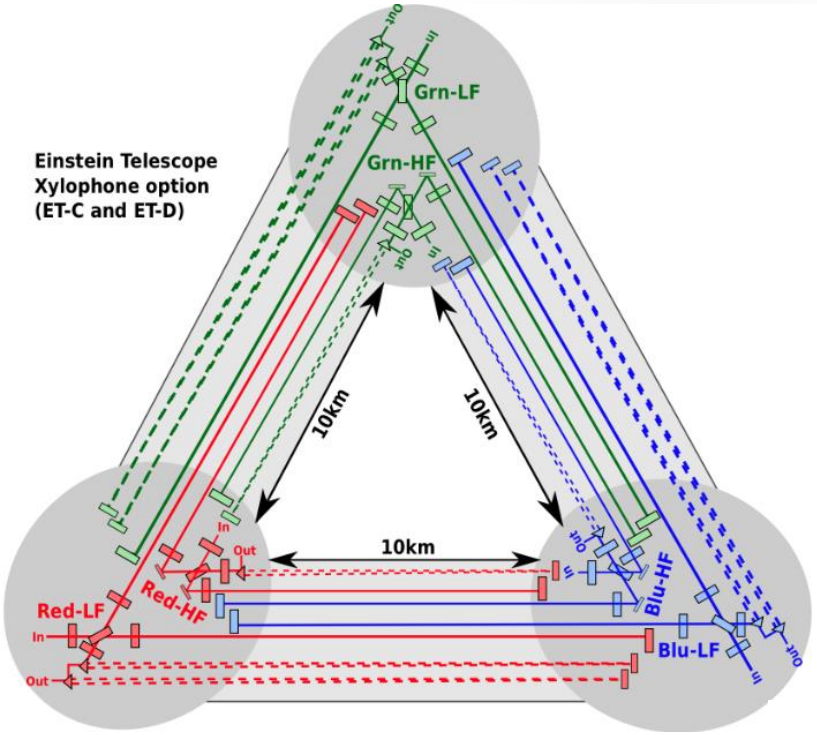

Conclusions

Advanced detectors:

- 50 confirmed CBC detections (GWTC-2), and more to come with the results from O3b (GWTC-3);
- Significant contribution of Advanced Virgo to the network: 5 two-detectors event involving V1, 7 events with sky-localization (90% C.R.) smaller than 1% of the sky area;
- Application and development of state-of-the-art technologies in interferometer working principle and control;
- Advanced Data Analysis techniques, involving refined computational and statistical methods, including Machine Learning.

Advanced Virgo+:

- A significant part of the upgrades for phase I has been completed and their commissioning has started (early 2021);
- Aiming at locking the full interferometer in August 2021;
- Phase II: mirror production has started, optical design and large payload under construction.

Backup slides

Antenna pattern function and network alignment

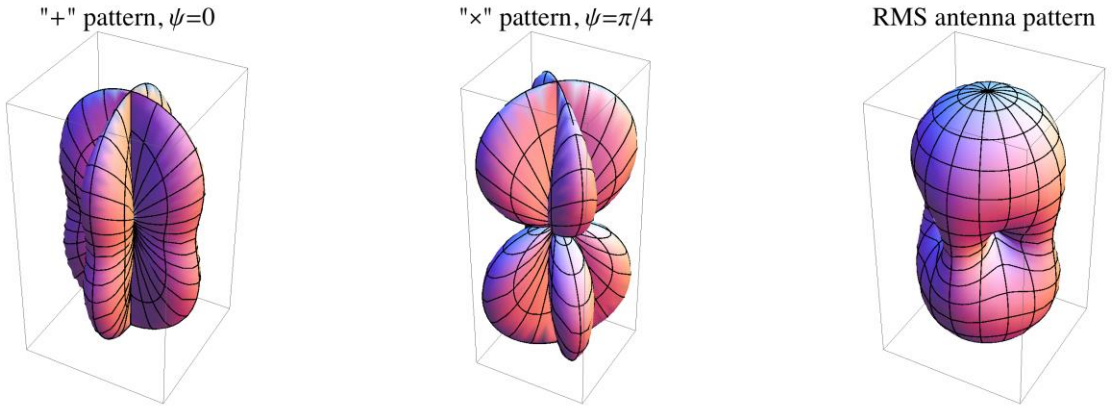

Network alignment: contribution to total network SNR from second polarization component. Important for reconstruction of both GW polarization and sky localization.

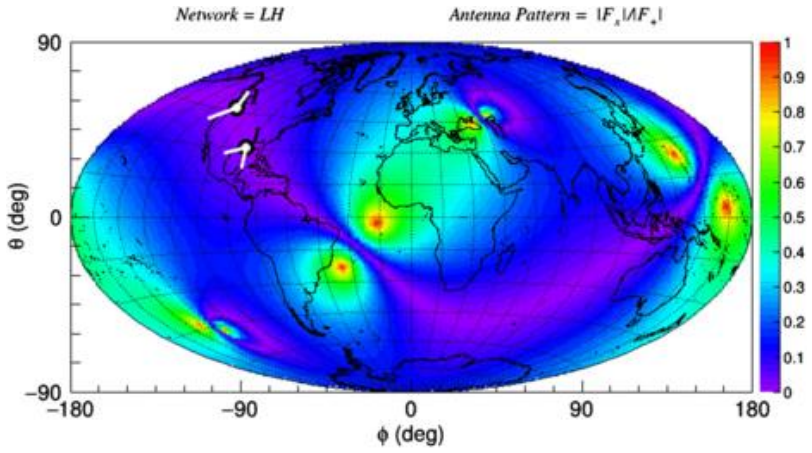

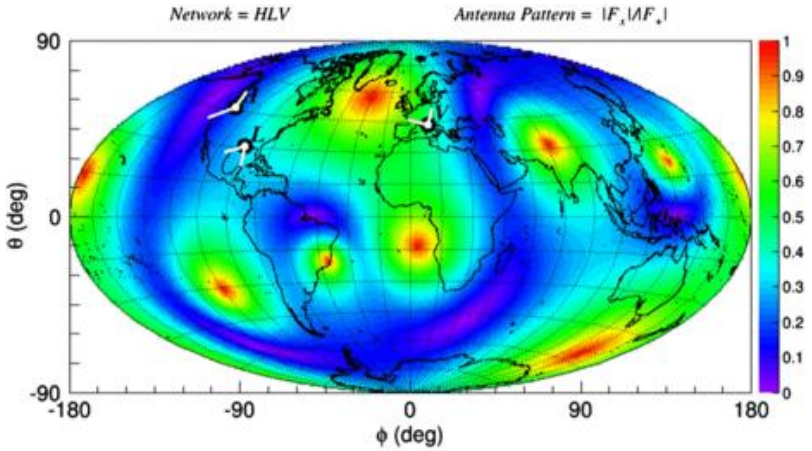

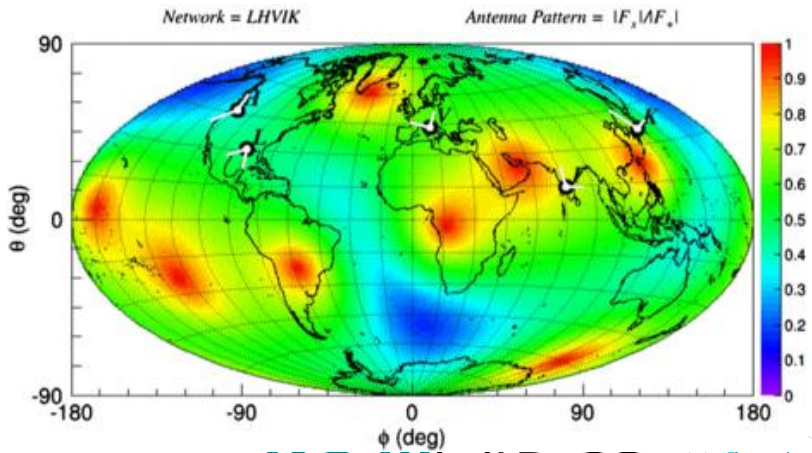

[Credit M. Drago]

O3a updated CBC rates

Population properties from the GWTC-2: arXiv:2010.14533

Differential rate density distribution of primary masses inferred using a Power Law + Peak model

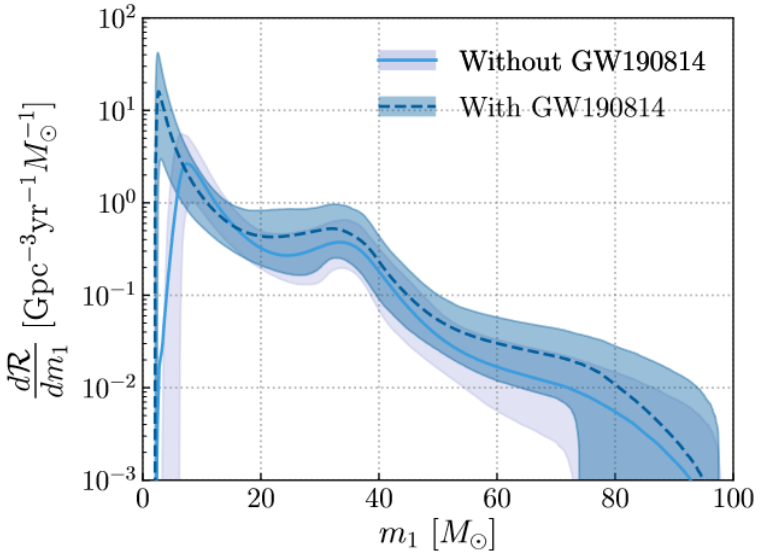

Merger rate density as a function of redshift

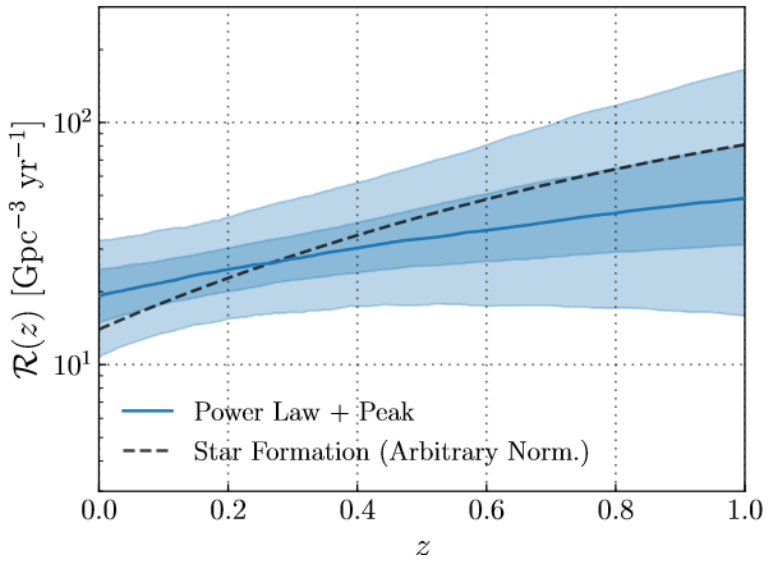

$$\mathcal{R}_{\mathrm{BNS}} = 320^{+490}_{-240}\ \mathrm{Gpc}^{-3}\ \mathrm{yr}^{-1}$$

$$\mathcal{R}_{\mathrm{BBH}} = 23.9^{+14.9}_{-8.6}\ \mathrm{Gpc}^{-3}\ \mathrm{yr}^{-1}$$

$$\mathcal{R}_{\mathrm{NSBH}} = 7^{+16}_{-6}\ \mathrm{Gpc}^{-3}\ \mathrm{yr}^{-1}\ *$$

* Assuming GW190814 is a NSBH